Snowmelt modeling using two melt-rate models in the Urumqi River watershed, Xinjiang Uyghur Autonomous Region, China

Muattar SAYDI[1,2] (iD) https://orcid.org/0000-0002-1982-6705; e-mail: muattar08@163.com

DING Jian-li[1,2*] (iD) https://orcid.org/0000-0002-2340-4492 ; ✉ e-mail: watarid@xju.edu.cn

Vasit SAGAN[3] (iD) https://orcid.org/0000-0003-4375-2096; e-mail: vasit.sagan@slu.edu

QIN Yan[1,2] (iD) https://orcid.org/0000-0002-0242-3272; e-mail: qinyan0215@163.com

* Corresponding author

1 College of Resource and Environmental Sciences, Xinjiang University, Urumqi 830046, China

2 Key Laboratory of Oasis Ecology, Xinjiang University, Urumqi 830046, China

3 Department of Earth and Atmospheric Sciences, Saint Louis University, St. Louis, MO 63108, USA

Abstract: In this paper, the performance of the classic snowmelt runoff model (SRM) is evaluated in a daily discharge simulation with two different melt models, the empirical temperature-index melt model and the energy-based radiation melt model, through a case study from the data-sparse mountainous watershed of the Urumqi River basin in Xinjiang Uyghur Autonomous Region of China. The classic SRM, which uses the empirical temperature-index method, and a radiation-based SRM, incorporating shortwave solar radiation and snow albedo, were developed to simulate daily runoff for the spring and summer snowmelt seasons from 2005 to 2012, respectively. Daily meteorological and hydrological data were collected from three stations located in the watershed. Snow cover area (SCA) was extracted from satellite images. Solar radiation inputs were estimated based on a digital elevation model (DEM). The results showed that the overall accuracy of the classic SRM and radiation-based SRM for simulating snowmelt discharge was relatively high. The classic SRM outperformed the radiation-based SRM due to the robust performance of the temperature-index model in the watershed snowmelt computation. No significant improvement was achieved by employing solar radiation and snow albedo in the snowmelt runoff simulation due to the inclusion of solar radiation as a temperature-dependent energy source and the local pattern of snowmelt behavior throughout the melting season. Our results suggest that the classic SRM simulates daily runoff with favorable accuracy and that the performance of the radiation-based SRM needs to be further improved by more ground-measured data for snowmelt energy input.

Keywords: Snowmelt runoff; Mountainous watershed; Urumqi River; Temperature; Radiation

Introduction

Runoff produced from seasonal snowmelt is an

important source of streamflow in many arid and semiarid watersheds around the world (Li and Williams 2008; Dou et al. 2011; Vicuña et al. 2011). Snow accumulation during cold seasons produces surface runoff during the melt season, providing water for drinking, irrigation and other uses (Boudhar et al. 2009; Jain et al. 2010). The timing and quantity of this water strongly depend on the occurrence of snowmelt (Brubaker and Rango 1996), which can be determined with hydrological models using detailed field observations (Martinec 1975; Dey et al. 1989; Zeinivand and De Smedt 2010; Verdhen et al. 2014; Karimi et al. 2016). Due to the rugged topography and extreme climate conditions of mountainous watersheds, field observations are often not readily available, therefore the necessary data required to run a hydrological model are difficult to obtain. Accurate modeling of watershed runoff in mountainous watersheds remains a challenge.

To this end, several watershed models have been developed to account for snowmelt with limited variables and parameters. The majority of these models range from empirical temperature-index models to physical energy-balance models (Hock 1999; Pellicciotti et al. 2005; Li and Williams 2008; Wu et al. 2011; Meng et al. 2015). Empirical temperature-index models have been widely used due to their flexibility in terms of data requirements (e.g. ability to run with temperature as the minimum model input) (Hock 2003; Pellicciotti et al. 2005; Zhang et al. 2007; Meng et al. 2015). Physical energy balance models capture the spatial variability in the hydrological processes throughout complex watersheds (Forbes et al. 2011); however, these models require more field-measured data for model parameterization (Brubaker and Rango 1996; Pellicciotti et al. 2005). To date, the performances of the two types of models have been investigated by researchers because their efficiencies are largely location dependent (WMO 1986; Rango and Martinec 1995; Verdhen et al. 2014; Azmat et al. 2016; Karimi et al. 2016).

Methods to improve snowmelt modeling performance by integrating empirical temperature-index approaches with the accuracy of physical energy-balance models have recently received much attention (Hock 1999; Pellicciotti et al. 2005; Li and Williams 2008). Much of these efforts have

been focused on either introducing new variables or parameters to the model calibrations or improving the calibrations of the model variables and parameters with new methods. An important model used for this purpose is SRM, which is one of the most widely used empirical temperature-index (degree-day) models, proven to be effective for snowmelt runoff simulations for data-sparse mountainous regions (Brubaker and Rango 1996; Xie et al. 2018). Despite much success of snowmelt modeling with SRM (Abudu et al. 2012), researchers still argue that the classic empirical temperature-index approach uses only temperature data for melt model computation and neglects solar radiation as a source of energy for snowmelt (Li and Williams 2008; Vafakhah et al. 2015).

To address this problem, attempts have been made to improve the surface melt-rate calculation by means of different melt models, and the classic temperature-index melt models were enhanced by incorporating shortwave solar radiation and snow albedo (Kondo and Yamazaki 1990; Hock 1999; Pellicciotti et al. 2005; Zeinivand and De Smedt 2010). The enhanced melt models were further employed by the classic SRM, and new algorithms for snowmelt discharge simulation have been developed (Li and Williams 2008; Verdhen et al. 2014; Vafakhah et al. 2015). Pellicciotti et al. (2005) proposed several radiation-based melt models and evaluated their accuracies through the separation of temperature-dependent and temperature-independent energy sources. A temperature-dependent radiation method proposed by Pellicciotti et al. (2005) was integrated into the melt-rate calculation of SRM (Li and Williams 2008) and employed to simulate the daily snowmelt runoff in a data-sparse, arid mountainous watershed of north western China. The results indicated that the enhanced SRM was capable of simulating daily streamflow and that it was highly sensitive to the watershed lapse rate used to extrapolate temperature and snow albedo, which determines the amount of available solar radiation for snowmelt (Li and Williams 2008). However, their study did not include the classic SRM. Further research is needed to account for the effects of the enhanced melt model on snowmelt modeling with a better watershed model.

Recently, the radiation-based SRM with net solar radiation suggested by Brubaker and Rango

(1996) was used in the Taleghan watershed, Iran (Vafakhah et al. 2015). Classic degree-day SRM and radiation-based SRM were developed to simulate daily snowmelt runoff. The results suggested that the radiation-based SRM outperformed the accuracy of the classic SRM due to the improved energy input algorithm. In contrast, different results were achieved by Verdhen et al. (2014), who evaluated the performances of the temperature-index and energy-balance models of SRM at a point-specific snowmelt computation in the western Himalayas. The results indicated that the uncertainties arose between different model performances, and the temperature-index algorithm of SRM holds a higher ranking in performance compared to its energy-balance version. Despite the significance of the surface energy balance in snowmelt processes (Hock 1999), the incorporation of radiation factors in the melt model is not always capable of yielding higher accuracy and better results. In addition, methods based on energy fluxes are often complex and not widely applicable because the necessary data are sparse (Hock 1999; Hock 2003). Therefore, the selection of a comparatively appropriate melt model is needed when daily runoff is computed with SRM, particularly in ungauged mountainous watersheds.

The objectives of this study are to (1) enhance the classic SRM by incorporating shortwave solar energy and compare the performances of temperature-index and radiation approaches in snowmelt modeling and (2) evaluate the effects of enhanced methods on improving the modeling accuracy of classic SRM in data-sparse mountainous watersheds.

1 Methods

In this section, the model of snowmelt simulation and essential melt model computation methods are presented. The classic SRM, which uses an empirical temperature-index approach and radiation-based SRM, integrated with solar radiation and snow surface albedo, are introduced.

1.1 SRM

Classic SRM calculates the runoff mainly by snowmelt and precipitation, with some additional deterministic parameters to describe the basin characteristics. The classic SRM computes the daily discharge of a basin using the following equation:

$$Q_{n+1} = [c_{sn} \cdot M_n \cdot S_n + c_{Rn} \cdot P_n] \\ \cdot \frac{A \cdot 10000}{86400}(1 - k_{n+1}) + Q_n \cdot k_{n+1} \quad (1)$$

where A is the area of the basin or zone (km²); k is the recession coefficient; and n is the sequence of days during the discharge computation period. In the SRM, the compositions of $c_{sn} \cdot M_n \cdot S_n$ and $c_{Rn} \cdot P_n$ account for the contributions of snowmelt and precipitation to the runoff, respectively; and 10000/86400 is the conversion from cm km² d⁻¹ to m³ s⁻¹ (conversion from runoff depth to discharge) (Martinec et al. 2008).

1.2 Melt models

Snowmelt computation of classic SRM is based on the temperature-index melt model. The melt rate is linearly related to air temperature, which is regarded as an integrated index of the total energy available for melt (Pellicciotti et al. 2005). Point-measured air temperature is extrapolated to different elevations of a watershed per elevation gradient (Martinec et al. 2008; Abudu et al. 2016; Saydi et al. 2017). Radiation-based SRM utilizes classic SRM (Equation 1) to calculate basin runoff and the same algorithm in temperature extrapolation. However, for the melt-rate calculation, radiation-based SRM incorporates the amount of melt water caused by temperature and shortwave solar energy computed with a temperature-dependent multiplicative formula (Pellicciotti et al. 2005；Li and Williams 2008). Equations 2 and 3 are the melt models for classic and radiation-based SRM, respectively.

$$M = \begin{cases} \alpha \cdot (T_d - T_0 + \Delta T_e) & T_d > T_0 \\ 0 & T_d \leq T_0 \end{cases} \quad (2)$$

$$M = \begin{cases} \alpha \cdot (T_d - T_0 + \Delta T_e) \cdot SRF \cdot (1-a) \cdot G & T_d > T_0 \\ 0 & T_d \leq T_0 \end{cases} \quad (3)$$

where M is the melt rate (cm d⁻¹); α is a degree-day factor (DDF) (cm °C⁻¹ d⁻¹); T_d is the daily mean temperature (°C); T_0 is the critical temperature above which snowmelt is assumed to occur (°C); ΔT_e is the adjusted values of temperature against elevation (°C); the daily value of $(T_d - T_0 + \Delta T_e)$

represents the numbers of daily available degree-days ($^{\circ}$C d^{-1}); *SRF* represents the solar radiation factor (m^2 d W^{-1}); *a* is the snow albedo, without units; and *G* is the incoming shortwave solar radiation (W m^{-2}).

In the classic SRM, new snow from a precipitation event is stored in the model and melted as soon as enough degree-days have occurred. In addition, the classic SRM keeps track of rainfall peaks per a certain amount of average daily rainfall in the watershed. However, the radiation-based SRM uses the critical temperature to decide whether snowmelt occurs and does not keep track of new snow and rainfall peaks (Martinec et al. 2008; Li and Williams 2008).

The altitude adjustment ΔT_e in Eqs. (2) and (3) is computed as follows:

$$\Delta T_e = \gamma \cdot (h_{st} - \bar{h}) \cdot \frac{1}{1000} \qquad (4)$$

where γ is the temperature lapse rate ($^{\circ}$C km^{-1}); and h_{st} and $\bar{h}$ are the altitude of the reference station and the hypsometric mean elevation for a given zone, respectively (Ma and Cheng 2003).

1.3 Solar radiation and snow albedo

Solar radiation over large areas is often estimated using sunshine hours or local meteorological data with additional atmospheric and topographic parameters (Liu and Jordan 1960; Kumar et al. 1997; Hofierka and Šúri 2002). The common problem with these statistical approaches is the estimation error manifested in the results interpolation or extrapolation from one site to other places. Satellite images also provide solar radiation calculations. However, satellite data are collected at discrete time intervals and therefore do not provide the continuous daily measurements required for modeling. Notably, radiation is strongly affected by topography and near ground features (Fu and Rich 1999). The solar analyst model is a highly optimized algorithm for radiation calculations based on DEM data. In this paper, clear-sky incoming shortwave solar radiation is calculated using a solar analyst in the ArcGIS platform based on a 30 m resolution DEM obtained from the United States Geological Survey (USGS). Global radiation, including direct plus diffuse radiation and omitting reflected radiation and possible cloud cover, was calculated daily for every 30 m pixel; the mean value of radiation within the watershed or a zone was determined as the global radiation value of the watershed or a given zone on a particular day (Fu and Rich 1999; Li and Williams 2008). More details about the solar analyst model implementation can be found in Fu and Rich (1999).

In a snow or ice-covered area, incoming shortwave radiation is strongly reflected. Snow albedo was introduced to determine the amount of shortwave radiation that is absorbed by the snow surface (Kondo and Yamazaki 1990; Roesch et al. 1999; Pellicciotti et al. 2005). Fresh snow albedo is approximately 0.86 and decays over time (Zeinivand and De Smedt 2010). In this paper, snow albedo is computed as an exponential function of accumulated days since the last fresh snowfall (Zeinivand and De Smedt 2010):

$$a_n = 0.43 \left[1 + \exp\left(-bt_{fn}\right) \right] \qquad (5)$$

where a_n is the albedo for the nth day since the last snowfall; *b* represents the rate of snow albedo decay (-0.2 d^{-1}); and t_{fn} is the time since the last fresh snow on the nth day. The value of t_f restarts ($t_f = 0$) with each fresh snowfall (Zeinivand and De Smedt 2010). The identified records for all snow or rain precipitation data can be used to determine the fresh snow day for the snow albedo calculation.

1.4 Snow cover area

Remote sensing observations are particularly useful for providing spatially detailed input data for snowmelt runoff modeling with relatively high spatial and temporal accuracy (Nagler et al. 2008). For a snow cover analysis, one of the most significant sensors is the Moderate Resolution Imaging Spectroradiometer (MODIS) onboard on both the Terra and Aqua satellites. The MODIS sensors operate with 36 narrow spectral bands that span from approximately 0.4-14.0 μm in the visible and thermal-infrared parts of the electromagnetic spectrum (Hall et al. 1995). Snow mapping with MODIS data is based on the normalized difference snow index (NDSI) algorithm and further exploits the unique nature of snow reflectance in the visible and near-infrared bands (Hall et al. 1995; Hall et al. 2002). Due to the robustness of the MODIS snow-

cover products, they are used worldwide and benefit hydrologists because the MODIS data have been improved for spatial resolution and geolocation accuracy and are readily available for users without further classification (Hall et al. 2002; Tekeli et al. 2005; Bilal et al. 2019). Currently, the MODIS snow products are distributed through the National Snow and Ice Data Center (NSIDC) at different spatial and temporal resolutions (Marcil et al. 2016; Han et al. 2019). The MODIS/Terra eight-day composites of global snow cover products at a 500-m spatial resolution were used in this paper. The MODIS data format was converted and projected to World Geodetic System 1984 (WGS84), Universal Transverse Mercator (UTM) using MODIS projection tool (MRT). There were 24 MOD 10A2 images available for each year from the beginning of March to the end of August at eight-day time intervals, and the images were mostly cloud-free. Daily snow cover data were obtained by the B-Spline interpolation method using successive images (Abudu et al. 2012).

2 Study Area and Data

For model calibration and validation, a mountainous watershed in the Urumqi River basin located in Xinjiang Uyghur Autonomous Region, China, was selected as the study area (Figure 1). Although glaciers exist in the target watershed, as rainfall and snowmelt together produce majority of the basin runoff (Saydi et al. 2017), the focus of this study is on the runoff simulation produced by snowmelt in the watershed, and meltwater due to snow and ice will not be distinguished in the following discussions. Moreover, the runoff produced from glacier melt mainly occurs in early summer (June and July) and is geographically limited to small areas (Xie et al. 2018).

2.1 The Urumqi River watershed

Snow and ice melt from the northern slopes of Tianshan Mountain in the Xinjiang Uyghur Autonomous Region of China feeds the regional streams in spring and summer. The Urumqi River begins at No. 1 Glacier near Tengri peak No. II on Tianshan Mountain. The river basin covers an area

of 4,684 km², which is located between 43°00′ to 44°07′ N latitude and 86°45′ to 87°56′ E longitude. The river flows northward from the mountain headwaters through the city of Urumqi and finally disappears in the northwestern part of the Gurbantunggut Desert. The Urumqi River has a total length of 214.3 km, with 62.6 km to the river outlet. Observational data from the Yingxiongqiao Hydrometric Station, located at the river outlet, between 1958 and 2012 show that the average annual runoff in the basin is 2.41×10^8 m³, the temperature is 1.7°C, and the annual precipitation is 454.5 mm; 69.2% of the annual runoff occurs during the summer season from June to August, and 52% of the annual precipitation is also concentrated during the same period (Saydi et al. 2013; Saydi et al. 2016). In the high mountainous area, the statistics of the Daxigou meteorological station from 1960 to 2012 indicate that the average annual temperature is -4.94°C, and the annual precipitation is 452.3 mm.

The Urumqi River watershed was delineated using DEM and GIS data, and a watershed area of approximately 1,074 km² was calculated. The selected watershed is further divided into four elevation zones (A, B, C and D) based on its physical characteristics and the available hydrometeorological data. The areas of each
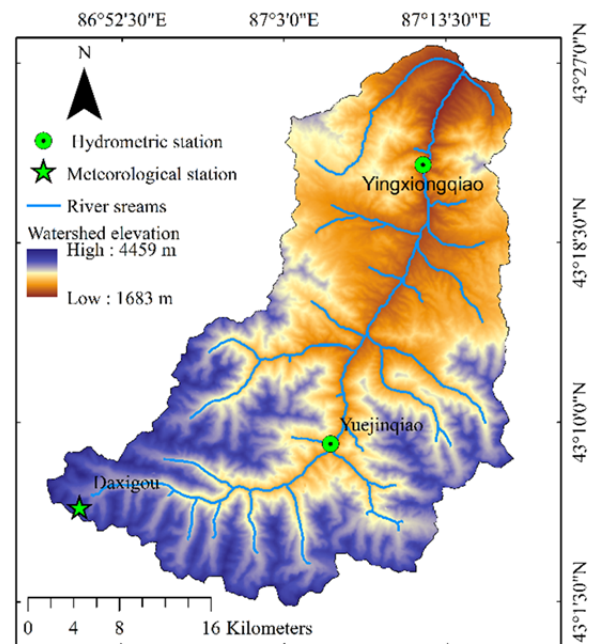
Figure 1 Location of the Urumqi River watershed. The base map, river streams and watershed boundary are derived from 30 m resolution DEM data.

Table 1 Hydrometeorological stations and data used in the Urumqi River watershed

Stations	Elevation	Location	Collected dataset and data scale
Yingxiongqiao	1920 m	87°12′ N 43°22′ E	Daily average temperature, runoff and precipitation over 2005-2012; monthly average temperature and precipitation over 1983-2012
Yuejinqiao	2313 m	87°06′ N 43°09′ E	Daily average temperature and precipitation over 2005-2012; monthly average temperature and precipitation over 1983-2012
Daxigou	3539 m	86° 49′ N 43° 06′ E	Daily average temperature and precipitation over 1960-2012

elevation zone were calculated to be 365.75 km², 263.32 km², 284.45 km² and 160.48 km² for zones A, B, C and D, respectively. There are two regular hydrometric stations established in the watershed. One station is located at the river outlet, Yingxiongqiao, and the other station is at the middle of the upper reach, Yuejinqiao. Data collected from the two hydrometric stations and one meteorological station, Daxigou, located at the high elevation upper end of the headwaters, were used. Zones A and B cover the areas located between Yuejinqiao and Yingxiongqiao, and the elevations range from 1680 to 3200 m with an average of 2600 m. Zones C and D have high elevations up to 4460 m with a mean of 3675 m and include all areas located between Yuejinqiao and Daxigou. The melt seasons of spring and summer from 2005 to 2012 were selected for runoff modeling. The models were calibrated to the years 2005-2007 and validated for 2008-2012. Table 1 shows the information about the three observation stations and data collection. Runoff and meteorological data from the two hydrometric stations were obtained from the Xinjiang Bureau of Hydrology and Water Resources, and the meteorological data from Daxigou meteorological station were provided by the National Meteorological Information Center of China.

2.2 Model inputs

The SRM uses air temperature, precipitation, and SCA as three essential variables to describe the basin hydrologic characteristics. Temperature and precipitation data from three stations are available and were extrapolated to the elevation zones. SCA can be extracted from satellite imagery. Model inputs were calibrated using the empirical relations and deterministic methods as described in the following section.

2.2.1 Temperature

As a principal variable of SRM, temperature affects the melting process of snow cover, and together with the critical temperature, it determines a precipitation event such as rain or snow (Rango and Martinec 1981; Abudu et al. 2012). For the classic SRM and radiation-based SRM, temperature data were recorded at three observation stations and extrapolated to the mean elevation of four zones by the lapse rates. Eq. 4 was used to calculate the adjusted value of temperature against elevation, and equations 2 and 3 were used to determine the numbers of total available degree-days and melt rates in each elevation zone. The lapse rate of the watershed was calculated using 30-year monthly average temperature data from three observation stations at different altitudes over the 1983-2012 period.

The results shown in Figure 2 suggest that the temperature decreased with elevation between the three stations over the melt season. Daxigou station at the highest altitude had the coolest settings, and the 30-year average melt season temperature was -0.3°C. Yuejinqiao and Yingxiongqiao stations at the lower elevations had relatively warm climates, and the 30-year average melt season temperatures were 6.7°C and 8.5°C, respectively. The melt temperature (usually above 0°C) occurred approximately a month earlier at Yingxiongqiao and Yuejinqiao than at Daxigou. Thus, snow melt in the lower and middle reaches of the watershed begins early in the spring, while the ablation process in the upper reach of the watershed begins later in the spring or early in the summer. Between Yingxiongqiao and Yuejinqiao, the lapse rate was relatively smaller in spring and began to increase in summer; the 30-year lapse rate averages varied from 0.1°C km⁻¹ to 6.5°C km⁻¹. The temperature lapse rates calculated between Yuejinqiao and Daxigou were relatively constant, and the 30-year mean lapse rates ranged from 5.3°C km⁻¹ to 6.0°C km⁻¹. For the model temperature input calculation, both the individual
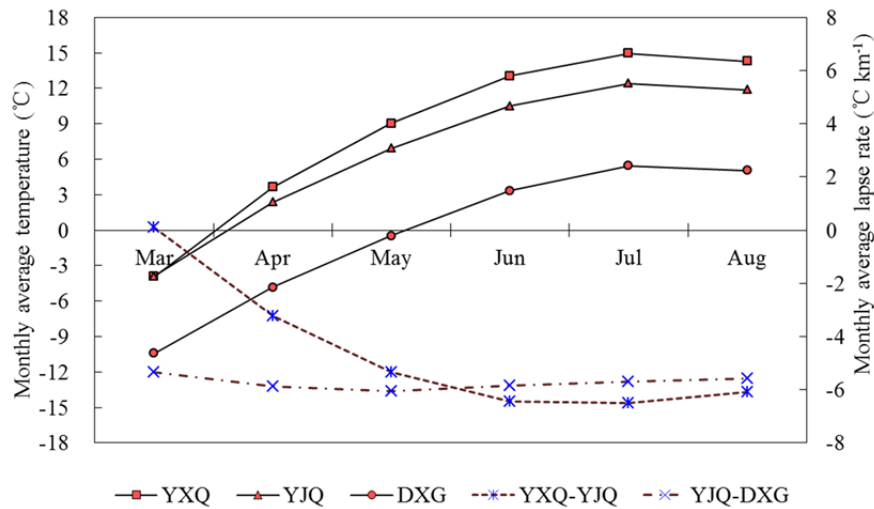
Figure 2 Thirty years of melt season average monthly temperatures and lapse rates in the Urumqi River watershed over the 1983-2012 period. YXQ, YJQ and DXG are the abbreviations for Yingxiongqiao, Yuejiqiao and Daxigou, respectively. YXQ-YJQ represents the lapse rate between Yingxiongqiao and Yuejinqiao; and YJQ-DXG represents the lapse rate between Yuejinqiao and Daxigou. The X axis represents the months of the melt season. The right-Y axis represents the average of the 30-year lapse rate during the melt season, and the left-Y axis represents that of the 30-year monthly temperature over the melt season.

year's lapse rate and the 30-year average of the lapse rates were used to extrapolate the temperature data. The results showed that the temperature extrapolated from the 30-year average lapse rates led to higher modeling accuracy. Thus, the 30-year average of the lapse rates and base station data were used to calculate the total available degree-days for snowmelt runoff modeling. The temperature in zone A was evaluated by the lapse rate between Yingxiongqiao and Yuejinqiao using Yingxiongqiao as a base station. For zone B, data from Yuejinqiao were used to extrapolate by the lapse rate between Yingxiongqiao and Yuejinqiao; for higher elevation zones C and D, the temperature records at Daxigou weather station were extrapolated to the mean elevation of each zone by the lapse rate between Yuejinqiao and Daxigou.

2.2.2 Precipitation

Precipitation is one of the major components of runoff, yet it is the most difficult to evaluate. In the watershed, precipitation contributes to annual discharge as much as snowmelt does (Saydi et al. 2017). Thus, the runoff modeling accuracy in the study watershed is closely related to the proper estimation of precipitation. Precipitation estimation in the study watershed mainly considers

the following three aspects:

First, the total amount of precipitation, seasonal distribution and precipitation gradient between the three stations were investigated using precipitation records and elevations. Statistics showed that over the melt season from 2005 to 2012, Daxigou had the greatest precipitation among all three stations, whereas Yuejinqiao had the smallest precipitation. The seasonal distribution of precipitation from 1983 to 2012 showed that in comparison to Yuejinqiao, Yingxiongqiao had greater precipitation in spring and smaller precipitation in summer. The 30-year average altitude gradient of precipitation from Yingxiongqiao to Yuejinqiao was -37.3 mm km^{-1} for spring and 17.7 mm km^{-1} for summer; for Yuejinqiao and Daxigou stations, the 30-year average altitude gradient of precipitation from Yuejinqiao to Daxigou was 2.3 mm km^{-1} for spring and 9.3 mm km^{-1} for summer.

Second, the correlations between basin runoff and precipitation from three hydrometeorological stations were monitored over the melt season from 2005 to 2012. The results showed that the precipitation from Daxigou was highly correlated with the watershed runoff; the eight-year average value of the correlation was 0.45. Additionally, there was a rather small correlation between the

watershed runoff and precipitation at Yingxiongqiao or Yuejinqiao, i.e., the eight-year values were 0.19 and 0.30, respectively. Therefore, the precipitation data from Daxigou were the most representative of the watershed precipitation behavior, and Daxigou was selected as a basic reference station for the precipitation extrapolation.

Finally, the possible combination of precipitation input from three stations was used to develop the best model. To cover all possible rainfall events in the middle and lower sections of the watershed and to obtain the maximum rainfall input during the flood season (July and August), the model precipitation data were further adjusted by the inclusion of precipitation records from Yingxiongqiao and Yuejinqiao stations (Saydi et al. 2016; Abudu et al. 2016).

2.2.3 Model parameterization

The recession coefficient k was a significant feature of SRM, and the runoff modeling performance was sensitive to the change in the recession coefficient (Martinec et al. 2008). In this paper, the recession coefficient was calculated with the runoff of no melt or rainfall during the recession by the following equation (Martinec et al. 2008; Li and Wang 2008; Saydi et al. 2016):

$$k_{n+1} = \frac{Q_{n+1}}{Q_n} = xQ_n^{-y} \qquad (6)$$

where Q_n and Q_{n+1} are recession discharges on n th and $(n+1)$ th day of the recession period, respectively; x and y are parameters of the recession coefficient.

A regression line was plotted to the logarithmic recession discharge over the calibration period of 2005-2007, and parameters x and y were further evaluated (Li and Wang 2008; Saydi et al. 2016).

Because of the lack of ground-measured data, the DDF was calculated by the empirical relationship between the DDF and snow density suggested by Martinec et al. (2008), and the snow density was referenced from related previous research outcomes in the Urumqi River basin (Yang et al. 1992; Hu 2004; Huang et al. 2007). The runoff coefficients of rain and snow were first initialized according to the basin characteristics and then adjusted against the modeling accuracy with an adjustment interval of 0.05 from 0.20 to 0.80. Critical temperature was set by the mean air

temperature and the precipitation records, which were defined as rainfall or snowfall (Saydi et al. 2016).

2.3 Model evaluation

The coefficient of determination (R^2) and volume difference (D_V) were used to assess model performances, and can be defined by the following equations:

$$R^2 = 1 - \frac{\sum_{i=1}^{n}(Q_i - Q_i')^2}{\sum_{i=1}^{n}(Q_i - \bar{Q})^2} \qquad (7)$$

where Q_i is the measured daily discharge; Q_i' is the computed daily discharge; $\bar{Q}$ is the average measured discharge over the snowmelt season; and n is the number of daily discharge values.

$$D_V[\%] = \frac{V_R - V_R'}{V_R}.100 \qquad (8)$$

where V_R is the measured runoff volume; and V_R' is the simulated runoff volume. The percent of D_V represents the overall prediction difference in the runoff volume.

3　Results and Discussion

3.1 Calibrated parameters

Calibrated model parameters for the four-zone classic and radiation-based SRM in the Urumqi River basin are specified in Table 2. All parameters, except the recession coefficients, were calibrated both spatially and temporally; the recession coefficients were calibrated basin-wide for the entire melt season.

3.2 Runoff simulation

For both the classic and radiation-based SRM, the melting season of spring and summer in 2005-2007 was used for calibration, and the same period of 2008-2012 was used for validation. Each model was performed using the parameters described in Table 2. The accuracy of the simulation is specified in Table 3, and the time-series comparisons of the measured and simulated daily runoff by the classic and radiation-based models are given in Figure 3.

Table 2 Model parameters calibrated for the snowmelt period of 2005-2007 for the classic SRM and radiation-based SRM

Parameters	Data input options	A (<2680 m)	B (2680-3200 m)	C (3200-3800m)	D (>3800 m)
Lapse rates (°C·km⁻¹)	by zone	March 0.10 April 3.20 May 5.40 June-July 6.50 August 6.10	March 0.10 April 3.20 May 5.40 June-July 6.50 August 6.10	March 5.30 April-May 6.00 June-July 5.80 August 5.60	March 5.30 April-May 6.00 June-July 5.80 August 5.60
Critical temperature (°C)	by zone	March-April 2.00 May 0.75 June-August 0	March 2.50 April-June 2.00 July-August 0.75	March-May 2.50 June 2.00 July-August 0.75	March-April 3.00 May 2.50 June 2.00 July-August 0.75
DDF (cm·°C⁻¹ d⁻¹)	by zone	March-June 0.15 July-August 0.22	March-April 0.15 May-June 0.22 July-August 0.24	March 0.22 April 0.24 June-May 0.26 July-August 0.28	March 0.24 April-May 0.26 June-August 0.28
Snow runoff coefficient	by zone	March 0.45 April 0.40 May 0.30 June 0.25 July 0.25 August 0.30	March 0.50 April 0.45 May 0.40 June-July0.35 August 0.40	March 0.55 April 0.50 May 0.45 June-July 0.45 August 0.50	March 0.55 April 0.50 May-July 0.45 August 0.50
Rain runoff coefficient	by zone	March 0.60 April 0.50 May-June 0.35 July-August 0.40	March 0.60 April 0.55 May-June 0.40 July-August 0.45	March- April 0.65 May 0.50 June 0.45 July-August 0.50	March-April 0.65 May 0.60 June 0.50 July-August 0.55
Recession coefficient	basin-wide	for entire snowmelt season x= 1.0101, y=0.076			
Base station		Yingxiongqiao	Yuejinqiao	Daxigou	Daxigou

The accuracy analysis showed that the results of both models were acceptable. For the simulation period, the average of R^2 for the classic SRM outperformed the radiation-based SRM, with a higher value of 0.81 in comparison to the lower value of 0.74; the radiation-based SRM yielded a smaller D_V of 3.31 than the D_V of 5.82 for the classic SRM. For the five-year validation period, the results of R^2 and D_V with the classic SRM ranged from 0.68 to 0.89 and 1.88 to 21.80, respectively; for the radiation-based SRM, the accuracy values of R^2 and D_V varied from 0.46 to 0.73 and 0.62 to 24.71, respectively; for the five-year average, the classic SRM showed a better performance, with an R^2 of 0.79 and D_V of 7.79, than the radiation-based SRM, with an R^2 of 0.63 and D_V of 10.58. Overall, for the 2005-2012 period, the average values of R^2 were 0.80 and 0.67, while the values of D_V were 7.05 and 7.86 for the classic and radiation-based SRM, respectively. Therefore, the accuracy of the classic SRM was higher than that of the radiation-based SRM. The observed and estimated discharges, as shown in Figure 3, illustrate that the estimated value of the daily snowmelt runoff with both models can characterize

Table 3 Snowmelt runoff modeling performance measures for the Urumqi River watershed with the classic and radiation-based SRM over the snowmelt period of 2005-2012

Period		Classic SRM		Radiation-based SRM	
		R^2	D_V(m³ s⁻¹)	R^2	D_V(m³ s⁻¹)
Calibration period	2005	0.80	5.44	0.71	6.05
	2006	0.77	7.65	0.73	1.20
	2007	0.85	4.38	0.77	2.69
Validation period	2008	0.75	1.89	0.71	2.23
	2009	0.89	7.69	0.46	17.34
	2010	0.68	21.80	0.53	24.71
	2011	0.79	1.88	0.73	8.02
	2012	0.85	5.70	0.72	0.62

Notes: Values of D_V are given in absolute values.

the general trend of the measured discharge during the melting season.

3.3 Discussion

The classic SRM used the temperature-index approach to estimate the snowmelt runoff and extrapolate the model variables against elevation, treating the temperature as the only source of melt energy. Radiation-based SRM managed to integrate the radiation and snow surface albedo

into the degree-day approach of melt water calculations and estimated the basin snowmelt as a combination of melt water caused by temperature and shortwave solar energy. Comparative studies between the temperature-index and radiation approaches showed that the performances of the temperature-index models were comparable to those of energy-balance models in daily snowmelt runoff modeling on the catchment scale (WMO 1998; Hock 1999), which was further confirmed by

our results.

As presented in Table 3 and Figure 3, the calibration models showed better agreement between the computed and observed runoff, and the daily streamflow values simulated by the classic SRM were closer to the measured values than those of the radiation-based SRM. However, the validation models for both the classic and radiation-based approaches, in part, poorly captured the runoff in summer, for example, the
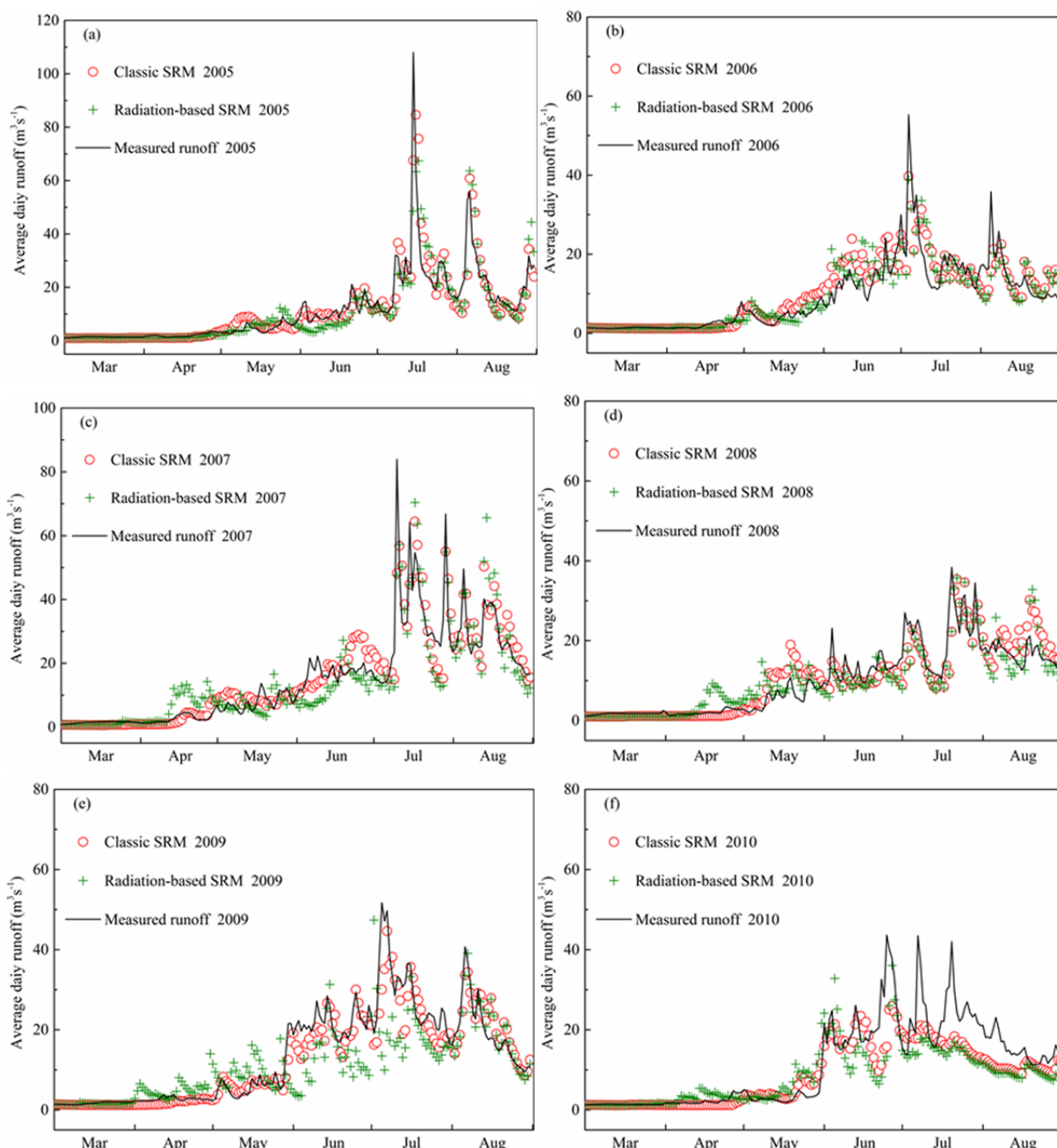
Figure 3 The observed and simulated daily runoff hydrographs using the classic SRM and radiation-based SRM at the Urumqi River watershed for 2005 to 2012. (-To be continued-)

(-Continued-)
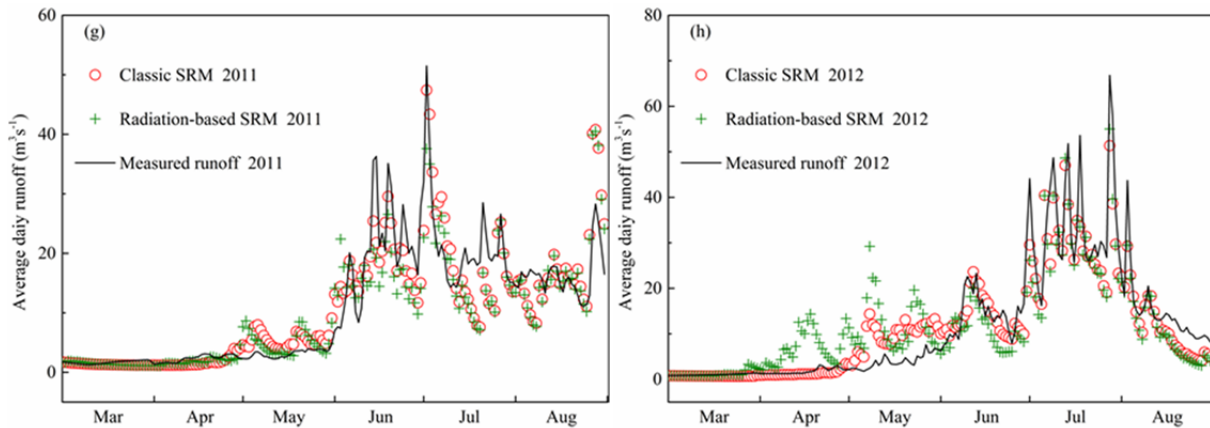
Figure 3 The observed and simulated daily runoff hydrographs using the classic SRM and radiation-based SRM at the Urumqi River watershed for 2005 to 2012.

hydrologic year of 2009-2010; the radiation-based model overestimated the runoff in late spring, such as April and May of 2009 and 2012; in addition, the estimated runoff matched each recession period well, except for the melt period of 2010 for the classic SRM and the melt period of 2009-2010 for the radiation-based model. Martinec and Rango (1986) noted that validation models that use calibrated parameters generally perform less well during years when conditions are not similar to those prevailing in the period used for calibration. The irregularity of the model variables in space and time also leads to less favorable results for model validation (Martinec and Rango 1986). In the Urumqi River watershed, the variation in precipitation was obvious over space and time. For example, the hydrologic year of 2010 had the least precipitation over the melting season, and the total available precipitation was 24% less than the average of the eight-year precipitation; an average of 50% of the total melt season precipitation was concentrated in the flood period over the other seven years, while only 33% of precipitation occurred in the flood season of 2010. This result could be considered as one of the possible reasons for the inaccuracy in the hydrological year of 2010 for both the classic and radiation-based models.

In the watershed studied in this paper, the melting accelerated slowly due to increased air temperature at the early stage of the melting season (spring), and the basin runoff was augmented by the snowmelt as the snow cover area shrinks. The snow cover data analysis showed that zone A was mostly snow free; zone B had snow

cover in the spring that melted before the summer arrived; zones C and D were partially covered by seasonal snow over the entire melt period and were also characterized by rapid snowmelt; and the eight-year averages of SCA at the end of spring were 19% and 38% for zone C and D, respectively. As summer begins, temperature increases, and the daily discharge begins to rise drastically due to the intense rainfall events in the mountainous area. However, both models underestimated the peak value of daily discharge during the flood season. This underestimation may be attributed to 1) the average SCA ratio obtained during the flood period over an eight year period being small, ranging from approximately 2-13% with an average of 7%; 2) melt water being reduced due to the diminished snow cover area and a discharge that was barely sufficient to cause flash floods, which is further confirmed by the discharge over the flood period caused by rainfall; and 3) the local intense rainfall events over the flood period not being measured, or perhaps not being precisely recorded by the available hydrological and meteorological stations in the watershed, where the streamflow was characterized by a rapid response. Therefore, the computed discharge failed to capture precisely the peak values of discharge. Moreover, the SRM was designed to simulate and forecasted daily discharges where snowmelt was a major runoff factor. However, in the Urumqi River watershed, the contribution of precipitation to runoff was greater than that of snowmelt, and other components, such as glacier melt and a small amount of groundwater, also contribute to

watershed discharge (Saydi et al. 2017). This attribute of the watershed was another factor that reduced model performance. Notably, glacial melt was not separately tracked in this study, and this may also have contributed to the decline of modeling accuracy in the Urumqi River watershed.

In comparison to the classic model, the radiation-based SRM performed less favorably, and no significant improvement was achieved by employing the solar radiation and snow albedo in the melt model calculation. Why was the inclusion of solar radiation not able to improve the modeling accuracy? To our knowledge, this can be explained by the following reasons.

The first reason is that the melt model used in the radiation-based SRM is temperature-dependent (Pellicciotti et al. 2005). The inclusion of solar energy was not calculated as an independent energy source to cause snowmelt; no melt was calculated below the critical temperature. In the Urumqi River watershed, at the early stage of snowmelt, there was usually enough snow-covered area, but the temperature was well below the critical temperature and no melt water was produced by including shortwave solar energy; at the later stage of snowmelt, in the late summer, the snow-covered area reduced sharply, and the inclusion of absorbed surface solar energy made a small difference in the melt process.

The second reason is that the computed distributed value of solar radiation over each zone was averaged daily without fully considering the actual distribution of solar radiation in snow-covered and snow-free areas. This may have caused over or underestimation of the incoming shortwave solar radiation, which contributes to the production of melt water from the SCA. The SRF was deterministically defined. The value of SRF was systematically varied, and the corresponding modeling accuracy was recorded. A deviation from the optimal value resulted in a considerable decline in the model accuracy, and the final value of the SRF was set to 0.00045 m² d W⁻¹. The α was also computed for clear-sky conditions, neglecting the influence of cloud cover. In addition, the calculated shortwave solar radiation based on the DEM was not validated due to the lack of measured radiation data in the watershed.

4 Conclusion

In this paper, the performance of the classic SRM was evaluated using two different melt models for snowmelt computation in the mountainous watershed of the Urumqi River over the snowmelt period of 2005 to 2012. The results indicate that both the temperature-index and radiation melt models demonstrated relatively good performances. The model parameters calibrated for the 2005-2007 snowmelt period are mostly stable for the next five-year validation period and can be regarded as representative of the basin characteristics. The classic SRM outperformed the radiation-based SRM due to the robust performance of the temperature-index model in the data sparse watershed. The radiation-based SRM simulated snowmelt runoff in the watershed with acceptable performance, as demonstrated by the eight-year average modeling accuracy of R^2=0.67 and D_V=7.86, which were lower than the classic SRM values of R^2=0.80 and D_V=7.05. Possible causes of the lower accuracy were the inclusion of solar radiation as a temperature-dependent energy source and the watershed snowmelt behavior throughout the melting season. Further efforts are needed to improve the accuracy of radiation-based SRM in this watershed by more rigorous parameterization and *in situ* radiation data to evaluate snowmelt energy.

United States Geological Survey (USGS) and National Snow and Ice Data Center (NSIDC)

Distributed Active Archive Center (DAAC).

References

Abudu S, Cui C, Saydi M, et al. (2012) Application of snowmelt runoff model (SRM) in mountainous watersheds: A review. Water Science and Engineering 5(2): 123-136. https://doi.org/10.3882/j.issn.1674-2370.2012.02.001

Azmat M, Choi M, Kim TW, et al. (2016) Hydrological modeling to simulate streamflow under changing climate in a scarcely gauged cryosphere catchment. Environmental Earth Sciences 75: 186. https://doi.org/10.1007/s12665-015-5059-2

Abudu S, Sheng Z, Cui C, et al. (2016) Integration of aspect and slope in snowmelt runoff modeling in a mountain watershed. Water Science and Engineering 9(4): 265-273. https://doi.org/10.1016/j.wse.2016.07.002

Brubaker KL, Rango A (1996) Response of snowmelt hydrology to climate change. Water Air and Soil Pollution 90(1-2): 335-343. https://doi.org/10.1007/BF00619293

Boudhar A, Hanich L, Boulet G, et al. (2009) Evaluation of the snowmelt runoff model in the Moroccan High Atlas Mountains using two snow-cover estimates. Hydrological Science Journal 54(6): 1094-1113. https://doi.org/10.1623/hysj.54.6.1094

Bilal H, Chamhuri S, Mazlin BM, et al. (2019). Recent snow cover variation in the Upper Indus Basin of Gilgit Baltistan, Hindukush Karakoram Himalaya. Journal of Mountain Science 16(2): 296-308. https://doi.org/10.1007/s11629-018-5201-3

Dou Y, Chen X, Bao A, et al. (2011) The simulation of snowmelt runoff in the ungauged Kaidu River Basin of TianShan Mountains, China. Environmental Earth Sciences 62(5): 1039-1045. https://doi.org/10.1007/s12665-010-0592-5

Dey B, Sharma VK, Rango A (1989) A test of snowmelt-runoff model for a major river basin in Western Himalayas. Hydrology Research 20(3): 167-178. https://doi.org/10.2166/nh.1989.0013

Forbes KA, Kienzle SW, Coburn CA, et al. (2011) Simulating the hydrological response to predicted climate change on a watershed in southern Alberta, Canada. Climatic Change 105(3-4): 555-576. https://doi.org/10.1007/s10584-010-9890-x

Fu P, Rich PM (1999) Design and implementation of the Solar Analyst: an ArcView extension for modeling solar radiation at landscape scales. Proceedings of the Nineteenth Annual ESRI User Conference, San Diego USA.

Hock R (1999) A distributed temperature-index ice-and snowmelt model including potential direct solar radiation. Journal of Glaciology 45(149): 101-111. https://doi.org/10.1017/s0022143000003087

Hall DK, Riggs GA, Salomonson VV (1995) Development of methods for mapping global snow cover using Moderate Resolution Imaging Spectroradiometer data. Remote Sensing of Environment 54(2): 127-140. https://doi.org/10.1016/0034-4257(95)00137-P

Hock R (2003) Temperature index melt modelling in mountain areas. Journal of Hydrology 282(1-4), 104-115. https://doi.org/10.1016/S0022-1694(03)00257-9

Hall DK, Riggs GA, Salomonson VV, et al. (2002) MODIS snow-cover products. Remote Sensing of Environment 83(1-2): 181-194. https://doi.org/10.1016/S0034-4257(02)00095-0

Hu R (2004) Physical Geography of the Tianshan Mountains in China. China Environmental Science Press. pp 140-233. (In Chinese)

Huang W, Huang Z, Cui C. (2007) Temporal and spatial distribution of snow density and its characteristics in Xinjiang. Journal of Glaciology and Geocryology 29(1): 66-71. (In Chinese) https://doi.org/10.3969/j.issn.1000-0240.2007.01.011

Han P, Long D, Han Z, et al. (2019) Improved understanding of snowmelt runoff from the headwaters of China's Yangtze River using remotely sensed snow products and hydrological modeling. Remote Sensing of Environment 224: 44-59. https://doi.org/10.1016/j.rse.2019.01.041

Jain SK, Goswami A, Saraf AK (2010) Assessment of snowmelt runoff using remote sensing and effect of climate change on runoff. Water Resources Management 24(9): 1763-1777. https://doi.org/10.1007/s11269-009-9523-1

Hofierka J, Šúri M (2002) The solar radiation model for Open source GIS: implementation and applications. Proceedings of the Open source GIS - GRASS users' conference, Trento Italy, September 2002.

Karimi H, Zeinivand H, Tahmasebipour N, et al. (2016) Comparison of SRM and WetSpa models efficiency for snowmelt runoff simulation. Environmental Earth Sciences 75: 664. https://doi.org/10.1007/s12665-016-5490-z

Kondo J, Yamazaki T (1990) A Prediction model for snowmelt, snow surface temperature and freezing depth using a heat balance method. Journal of Applied Meteorology 29: 375-384. https://doi.org/10.1175/1520-0450(1990)029<0375:APMFSS>2.0.CO;2

Kumar L, Skidmore AK, Knowles E (1997) Modeling topographic variation in solar radiation in a GIS environment. International Journal of Geographic Information Science 11(5): 475-497. https://doi.org/10.1080/136588197242266

Li X, Williams MW (2008) Snowmelt runoff modeling in an arid mountain watershed, Tarim Basin, China. Hydrological Processes 22(19): 3931-3940. https://doi.org/10.1002/hyp.7098

Liu B, Jordan RC (1960) The interrelationship and characteristic distribution of direct, diffuse and total solar radiation. Solar Energy 4(3): 1-19. https://doi.org/10.1016/0038-092X(60)90062-1

Li H, Wang J. (2008) The snowmelt runoff model applied in the Upper Heihe River Basin. Journal of Glaciology and Geocryology 30(5): 769-775. (In Chinese) http://ir.casnw.net/handle/362004/11922

Ma H, Cheng G (2003) A test of snowmelt runoff model (SRM) for the Gongnaisi River basin in the western Tianshan Mountainous, China. Chinese Science Bulletin 48(20): 2253-2259. https://doi.org/10.1007/BF03182862

Martinec J (1975) Snowmelt runoff model for stream flow forecasts. Hydrology Research 6(3): 145-154. https://doi.org.10.2166/nh.1975.0010

Martinec J, Rango A, Roberts RT (2008) Snowmelt Runoff Model (SRM) User's Manual. New Mexico State University Press. pp 19-39.

Martinec J, Rango A (1986) Parameter Values for Snowmelt Runoff Modelling. Journal of Hydrology 84(3-4): 197-219. https://doi.org/10.1016/0022-1694(86)90123-X

Marcil GK, Trudel M, Leconte R (2016) Using Remotely Sensed MODIS Snow Product for the Management of Reservoirs in a Mountainous Canadian Watershed. Water Resources Management 30(8): 2735-2747. https://doi.org/10.1007/s11269-016-1319-5

Meng X, Yu D, Liu Z (2015) Energy Balance-Based SWAT Model to Simulate the Mountain Snowmelt and Runoff – Taking the Application in Juntanghu Watershed (China) as an Example. Journal of Mountain Science 12(2): 368-381. https://doi.org/10.1007/s11629-014-3081-6

Nagler T, Rtto H, Malcher P, et al. (2008) Assimilation of meteorological and remote sensing data for snowmelt runoff forecasting. Remote Sensing of Environment 112(4): 1408-1420. https://doi.org/10.1016/j.rse.2007.07.006

Pellicciotti F, Brock B, Strasser U, et al. (2005) An enhanced temperature-index glacier melt model including the shortwave radiation balance: Development and testing for Haut Glacier d'Arolla, Switzerland. Journal of Glaciology 51(175): 573-587. https://doi.org/10.3189/172756505781829124

Rango A, Martinec J (1995) Revisiting the degree-day method for snowmelt computations. Journal of the American Water Resources Association 31(4): 657-669. https://doi.org/10.1111/j.1752-1688.1995.tb03392.x

Roesch A, Gilgen A, Wild M, et al. (1999) Assessment of GCM simulated snow albedo using direct observations. Climate Dynamics, 15(6): 405-418. https://doi.org/10.1007/s003820050290

Rango A, Martinec J (1981) Accuracy of snowmelt runoff simulation. Nordic Hydrology 12(4-5): 265-274. https://doi.org/10.2166/nh.1981.0021

Saydi M, Abudu S, Cui C, et al. (2013) Hydrological characteristics of typical watersheds in North Tianshan. Journal of China Hydrology 33(2): 87-92. (In Chinese) https://doi.org/10.3969/j.issn.1000-0852.2013.02.018

Saydi M, Ding J, Abudu S, et al. (2016) Simulation of snowmelt runoff in the northern slope of Tianshan mountains. Arid Zone Research 33(3): 636-642. (In Chinese) https://doi.org/10.13866/j.azr.2016.03.25

Tekeli AE, Akyürek Z, Şorman A (2005) Using MODIS snow cover maps in modeling snowmelt runoff process in the eastern part of Turkey. Remote Sensing of Environment 97(2): 216-230. https://doi.org/10.1016/j.rse.2005.03.013

Vicuña S, Garreaud RD, Mcphee J (2011) Climate change impacts on the hydrology of a snowmelt driven basin in semiarid Chile. Climatic Change 105(3-4): 469-488. https://doi.org/10.1007/s10584-010-9888-4

Verdhen A, Chahar BR, Sharma OP (2014) Snowmelt modelling approaches in watershed models: computation and comparison of efficiencies under varying climatic conditions. Water Resources Management 28(11): 3439-3453. https://doi.org/10.1007/s11269-014-0662-7

Vafakhah M, Nouri A, Alavipanah SK (2015) Snowmelt-runoff estimation using radiation SRM model in Taleghan watershed. Environmental Earth Sciences 73(3): 993-1003. https://doi.org/10.1007/s12665-014-3449-5

Wu L, Li H, Wang L (2011) Application of a degree -day model for determination of mass balance of Urumqi Glacier No.1, Eastern Tianshan, China Journal of Earth Science 22(4): 470-481. https://doi.org/10.1007/s12583-011-0201-x

World Meteorological Organization (WMO) (1986) Intercomparison of models of snowmelt runoff. Geneva Switzerland, World Meteorological Organization.

Xie S, Du J, Zhou X, et al. (2018) A progressive segmented optimization algorithm for calibrating time-variant parameters of the snowmelt runoff model (SRM). Journal of Hydrology 566: 470-483. https://doi.org/10.1016/j.jhydrol.2018.09.030

Yang D, Zhang Y, Zhang Z (1992) A Study on the Snow Density in the Head Area of Urumqi River Basin. Acta Geographica Sinica 3: 260-266. (In Chinese) https://doi.org/10.11821/xb199203007

Zeinivand H, de Smedt FD (2010) Prediction of snowmelt floods with a distributed hydrological model using a physical snow mass and energy balance approach. Natural Hazards 54(2): 451-468. https://doi.org/10.1007/s11069-009-9478-9

Zhang Y, Liu S, Ding Y (2007) Glacier meltwater and runoff modelling, Keqicar Baqi glacier, southwestern Tien Shan, China. Journal of Glaciology 53(180): 91-98. (In Chinese) https://doi.org/10.3189/172756507781833956